Vibrational excitons in α-helical polypeptides: Multiexciton self-trapping and related infrared transient absorption

Dmitry V. Tsivlin[a)]
Institut für Physik, Humboldt-Universität zu Berlin, Newtonstraße 15, D-12489 Berlin, Federal Republic of Germany

Hans-Dieter Meyer
Theoretische Chemie, Universität Heidelberg, Im Neuenheimer Feld 229, D-69120 Heidelberg, Federal Republic of Germany

Volkhard May
Institut für Physik, Humboldt-Universität zu Berlin, Newtonstraße 15, D-12489 Berlin, Federal Republic of Germany

(Received 12 December 2005; accepted 3 February 2006; published online 6 April 2006)

Based on the multiexciton expansion of a model Hamiltonian, an accurate quantum-dynamical description of vibrational states formed by amide modes in α-helical polypeptides is presented. Using the multiconfiguration time-dependent Hartree method, linear and pump-probe infrared absorption spectra are calculated by numerical time propagation of the exciton-chain vibrational wave function. The formation of self-trapped exciton states is discussed within the approximation of adiabatic excitons and within the full quantum description. © *2006 American Institute of Physics*. [DOI: 10.1063/1.2180247]

I. INTRODUCTION

The improvements of infrared spectroscopy achieved at the end of the 1990s initiated various new studies, in particular, by introducing the concept of two-dimensional spectroscopy.[1–3] Emphasis has been put on the investigation of small peptides where a direct excitation of the various amide group vibrations by infrared photons is possible. Noting the mutual coupling of the amide group vibrations and their possible delocalization (see, for example, Refs. 4 and 5), ultrafast two-dimensional spectroscopy has been considered as a tool to elucidate the conformation even of small proteins.

In particular, these developments reanimated the long-standing debate on the existence or nonexistence of the so-called Davydov solitons. By that one means the coherent motion of self-trapped amide vibrations through an α-helical polypeptide. Self-trapping has been proposed via a coupling of the amide excitations to low-frequency helix vibrations. Since the pioneering work of Davydov, this problem has been extensively studied theoretically (see Ref. 6 for an overview). However, an experimental proof for the existence of self-trapped states in α helices has been lacking until recently.[7]

In α-helical polypeptides, a sequence of amide units (–CONH–) forms the helical structure, which is stabilized by three quasilinear strands of hydrogen bonds. The local amide modes, such as C═O or N-H stretching mode, positioned at different units may be coupled by electrostatic interactions, in this way forming delocalized excited states, i.e., vibrational Frenkel excitons. Modulation of the amide mode frequencies via a deformation of the hydrogen bonds introduces a nonlinear coupling term, which favors self-trapping of the excitation. Evidence of exciton self-trapping has been found in peptide model crystals built of organic molecular chains stabilized by hydrogen bonding.[8,9] And recently, as already mentioned, infrared pump-probe experiments for dissolved α-helical polypeptides have been carried out, too. Applying ultrafast infrared pump-probe spectroscopy Ref. 7 announced the observation of a N-H stretching mode self-trapping in the poly-γ-benzyl-*L*-glutamate helix. Two positive bands in the transient absorption spectrum have been assigned to self-trapped two-exciton states.

In typical α-helical polypeptides the characteristic bandwidth of the vibrational excitons is smaller than the cutoff frequency of the longitudinal chain vibrations, which has been pointed out, for example, in Ref. 10. Hence, in principle, a quantum description of both the amide excitations and helix vibrations is required. In order to achieve the quantum-dynamical description of the configurational coordinates, a simplified form of the Hamiltonian has been used since the early days of this research (cf. Ref. 11). It employs a mapping of the peptide units along one strand of hydrogen bonds onto a one-dimensional chain of quantum harmonic oscillators. Exciton self-trapping in this model has been extensively studied using the so-called Davydov ansatz for the respective wave function.[12–14] Recently, it was suggested[15–17] that the intrinsic anharmonicity of amide modes plays an important role when more than one amide excitation is present. Since the energy of an amide double excitation is reduced in the anharmonic case, two excitons do not move independently, but rather form a bound self-trapped state.[15]

Electronic structure calculations using, for example, the density functional theory have been carried out only in recent

[a)]Electronic mail: tsivlin@physik.hu-berlin.de

years but concentrating on small oligopeptides.[4,5,18] From such types of calculations a series of parameters applied to the excitonic model of polypeptides with hydrogen bonding has been deduced in Refs. 4 and 5. This approach has been used to identify the two-dimensional (2D) infrared spectra of model α- and 3_{10}-helical structures.[4] However, since these studies were aimed to distinguish between the signatures of different polypeptide conformations, they were done for fixed configurations of amide units.

To study the equilibrium properties of flexible α-helical polypeptides quantum Monte Carlo simulations can be used.[19,20] This technique is not restricted by formal approximations and the accuracy is limited only by the finite grid size and statistical errors. In the nonequilibrium case, time propagation of a multidimensional wave function is required. The computational effort for such calculations scales exponentially with the number of dimensions. However, the numerical efficiency can be significantly improved by the use of the multiconfiguration time-dependent Hartree (MCTDH) method.[21–24] Here, the wave function is expanded in the basis of time-dependent products of single coordinate wave functions (Hartree products). Based on the Dirac-Frenkel variational principle, equations of motion are formulated for the expansion functions and for the expansion coefficients. Since the expansion functions depend on time, they may be adapted to the full wave function and thus drastically reduced in their overall number.[24]

In the present paper, amide exciton dynamics and related linear and transient infrared absorption spectra are studied by this MCTDH method. As was pointed out in Ref. 5, the amide I (C═O stretching) mode is well suited to introduce a simple Frenkel-exciton model, whereas in the case of the amide A mode (N-H stretch) this would be complicated by a Fermi resonance with the overtone of the amide II mode. Therefore, we consider a model exciton Hamiltonian taking into account the amide I mode only and applying a one-dimensional chain model of the α helix. The concrete type of peptide is of less importance for the following calculations (it only enters via the chain masses and concrete amide I mode excitation energies).

The full exciton-chain vibrational wave function for systems with at least ten amide units is constructed using a multiexciton expansion of the model Hamiltonian.[25] The resulting linear absorption spectra are tested against the exact MCTDH calculations, which explicitly account for the amide coordinates. Although the presented description of the complete exciton vibrational quantum dynamics requires some simplifications with respect to the structure and possible excitations in real α-helical polypeptides, we believe that the key effects are accounted for. In this way the present treatment fills the gap between calculations on exciton levels in long chains, ignoring any chain motion and *ab initio* considerations of di- or tripeptides.[4,5,18] We also consider the treatment given here as a description which is conceptually easier than that of Refs. 15–17, but also allows one to calculate linear and transient infrared spectra in a very direct way based on a multiexciton chain vibrational wave packet propagation.

The paper is organized as follows. In the subsequent section we present the definition of the model Hamiltonian and its ordering with respect to the multiexciton states. The adiabatic single- and two-exciton states (together with a specification of the model) are introduced in Sec. III as a guideline for interpreting the infrared absorption spectra. Section IV describes the application of the MCTDH method for time propagation of the exciton-chain vibrational wave function. Results for the linear and transient absorption spectra are presented in Sec. V and some conclusions are drawn in Sec. VI. In the Appendix we present some matrix elements of the Morse oscillator which are used in the multiexciton expansion of the Hamiltonian and all respective matrix elements of the complete Hamiltonian.

II. THE MODEL

The general structure of the model we will use in the following is in line with the majority of all those which have been applied earlier to study exciton self-trapping (see Ref. 6). It is particularly oriented on what has been done in Refs. 15–17. Therefore, the Hamiltonian is based on a one-dimensional model (the chain model) of an α-helical polypeptide. However, we will avoid any second-quantization notation (cf., e.g., Refs. 15 and 16), but include the intrinsic anharmonicity of the amide modes. Moreover, besides a complete coordinate representation of the Hamiltonian we also introduce a multiexciton expansion of the amide unit part which we consider to be more flexible than the second-quantization description of anharmonicities. This approach also avoids the application of two types of canonical transformations introduced to remove the amide unit internal anharmonicity and to renormalize the coupling to the chain vibrations.

A. The basic Hamiltonian

First, we shortly introduce a rather general expression for the polypeptide Hamiltonian H_{mol}, which is sufficient to motivate and carry out the multiexcitation expansion. It includes the high-frequency excitations of the various amide units and their mutual electrostatic coupling via H_{amide}. The longitudinal vibrations of the chain are characterized by H_{chain}. The part H_{coup} accounts for the modulation of the amide unit excitations via the actual chain configuration. Finally, including the coupling to the radiation field via $H_{\mathrm{field}}(t)$ the expression for the complete Hamiltonian is given by

$$H(t) = H_{\mathrm{mol}} + H_{\mathrm{field}}(t) = H_{\mathrm{amide}} + H_{\mathrm{chain}} + H_{\mathrm{coup}} + H_{\mathrm{field}}(t). \tag{1}$$

To specify all parts of the Hamiltonian in somewhat more detail we count the amide units in the chain by m $(=1,\ldots,N)$. Their spatial position along the chain is fixed by the set of one-dimensional coordinates $x=\{x_m\}$ (transversal displacements with respect to the chain are neglected). There are different normal mode coordinates characterizing every amide unit m. As already mentioned, we only consider a single internal coordinate Q_m (amide I coordinate) per amide unit. This all results in

$$H_{\text{amide}} = \sum_m H_m + \sum_{m<n} V_{m,n}(Q_m, Q_n). \tag{2}$$

Here, H_m is a single amide unit Hamiltonian including the anharmonic potential $V_m(Q_m)$. The potentials $V_{m,n}$ describe the electrostatic coupling between the amide oscillators at different sites. Both types of potentials will be further specified in Sec. III A.

The part of the Hamiltonian describing the longitudinal motion of the chain of amide units is specified here as

$$H_{\text{chain}} = T_{\text{vib}} + U(x), \tag{3}$$

where $U(x)$ is the overall potential energy function describing the chain vibrations and x denotes the N-dimensional vector of the chain units. The modulation of the local amide oscillator potentials by the chain coordinates is described by the term

$$H_{\text{coup}} = \sum_m \Delta V_m(Q_m, x). \tag{4}$$

The quantities ΔV_m have to be understood as the chain-coordinate dependent corrections to the potentials V_m entering Eq. (2). Finally, we use the molecule field coupling in the standard dipole approximation

$$H_{\text{field}}(t) = -\mathbf{E}(t)\hat{\boldsymbol{\mu}}, \tag{5}$$

where $\mathbf{E}(t)$ denotes the external electric field and $\hat{\boldsymbol{\mu}}$ is the dipole operator covering all amide units. $\hat{\boldsymbol{\mu}}$ as well as H_{coup} will be further specified in Sec. III A.

B. Multiexcitation expansion

When carrying out infrared spectroscopy of amide group excitations at least the first overtone is excited. Thus a restriction to low vibrational excitations remains to be sufficient, which suggests an expansion with respect to the low lying states only.[1] This procedure is well known from the description of electronic Frenkel excitons (cf., for example, Refs. 26 and 27) and will be shortly repeated here. (Note also the similarity to the second Born-Oppenheimer approximation, popular in relation to simulations of proton transfer reactions, see, e.g., Ref. 26.)

As an expansion basis we use the eigenstates of the local amide oscillators, i.e., the solutions of the following stationary Schrödinger equations for the mth local oscillator:

$$H_m \chi_{m\mu}(Q_m) = E_{m\mu}\chi_{m\mu}(Q_m). \tag{6}$$

Here, $E_{m\mu}$ and $\chi_{m\mu}(Q_m)$ are the amide eigenenergy and eigenstate, respectively, corresponding to the quantum number μ $(=0,1,2,\ldots)$.

These states are used to introduce the product states of the amide units of the whole chain

$$|\{\mu_m\}\rangle = \prod_m \chi_{m\mu_m}(Q_m). \tag{7}$$

An ordering of the total Hamiltonian with respect to the number of amide vibrational excitations is obtained as follows. We start with the vibrational ground state $|0\rangle$ of the whole system:

$$|0\rangle = \prod_m \chi_{m0}(Q_m). \tag{8}$$

Then the states

$$|\phi_m\rangle = \chi_{m1}(Q_m)\prod_{n\neq m}\chi_{n0}(Q_n) \tag{9}$$

follow, describing the presence of a single amide vibration at site m brought into the first excited level. The presence of a single overtone at site m is denoted as

$$|\tilde{\phi}_{m,m}\rangle = \chi_{m2}(Q_m)\prod_{n\neq m}\chi_{n0}(Q_n). \tag{10}$$

A double excitation becomes also possible via the presence of two singly excited amide groups at site m and at site n

$$|\tilde{\phi}_{m,n}\rangle = \chi_{m1}(Q_m)\chi_{n1}(Q_n)\prod_{k\neq m,n}\chi_{k0}(Q_k). \tag{11}$$

Since $|\tilde{\phi}_{m,n}\rangle \equiv |\tilde{\phi}_{n,m}\rangle$, we set $m<n$ in Eq. (11).

For the present consideration a concentration on these types of excitations remains to be sufficient. The ground state and the respective manifolds of singly and doubly excited states should be characterized by projection operators labeled as $\hat{P}_0$, $\hat{P}_1$, and $\hat{P}_2$, respectively. The projector on the ground state is simply

$$\hat{P}_0 = |0\rangle\langle 0|. \tag{12}$$

The manifold of singly excited states is characterized by

$$\hat{P}_1 = \sum_m |\phi_m\rangle\langle\phi_m|, \tag{13}$$

and that of doubly excited states by

$$\hat{P}_2 = \sum_{m\leqslant n} |\tilde{\phi}_{m,n}\rangle\langle\tilde{\phi}_{m,n}|. \tag{14}$$

The expansion of the full Hamiltonian, Eq. (1), up to the manifold of doubly excited states follows as

$$H = H_0 + H_1 + H_2 + [H_{1,0} + H_{2,0} + H_{2,1} + \text{H.c.}]. \tag{15}$$

The Hamiltonian describing the chain motion in the ground state is defined as

$$H_0 = \hat{P}_0 H \hat{P}_0 = \langle 0|H_{\text{mol}}|0\rangle|0\rangle\langle 0|. \tag{16}$$

The coupled dynamics of a single amide excitation and the chain motion is characterized by

$$H_1 = \hat{P}_1 H \hat{P}_1 = \sum_{m,n}\langle\phi_m|H_{\text{mol}}|\phi_n\rangle|\phi_m\rangle\langle\phi_n|. \tag{17}$$

Respective double excitations and the chain motion are covered by

$$H_2 = \hat{P}_2 H \hat{P}_2 = \sum_{m\leqslant n}\sum_{k\leqslant l}\langle\tilde{\phi}_{m,n}|H_{\text{mol}}|\tilde{\phi}_{k,l}\rangle|\tilde{\phi}_{m,n}\rangle\langle\tilde{\phi}_{k,l}|. \tag{18}$$

Here, we assumed that the coupling to the radiation field does not contribute to the intramanifold expressions (all matrix elements of H_{mol} are time independent; for their explicit formulation see Appendix).

Intermanifold coupling follows from

$$H_{1,0}(t) = \hat{P}_1 H \hat{P}_0 = \sum_m \langle \phi_m | H | 0 \rangle | \phi_m \rangle \langle 0 |, \tag{19}$$

$$H_{2,0}(t) = \hat{P}_2 H \hat{P}_0 = \sum_{m \leqslant n} \langle \tilde{\phi}_{m,n} | H | 0 \rangle | \tilde{\phi}_{m,n} \rangle \langle 0 |, \tag{20}$$

$$H_{2,1}(t) = \hat{P}_2 H \hat{P}_1 = \sum_{m \leqslant n} \sum_k \langle \tilde{\phi}_{m,n} | H | \phi_k \rangle | \tilde{\phi}_{m,n} \rangle \langle \phi_k |. \tag{21}$$

These expressions include the expansion of the dipole operator entering $H_{\mathrm{field}}(t)$, Eq. (5), as follows:

$$\hat{\boldsymbol{\mu}} = \hat{P}_1 \hat{\boldsymbol{\mu}} \hat{P}_0 + \hat{P}_2 \hat{\boldsymbol{\mu}} \hat{P}_1 + \mathrm{H.c.} \equiv \hat{\boldsymbol{\mu}}_{1,0} + \hat{\boldsymbol{\mu}}_{2,1} + \mathrm{H.c.} \tag{22}$$

III. ADIABATIC VIBRATIONAL EXCITONS

For a proper interpretation of the complete quantum dynamics of the amide unit excitations coupled to the chain motion it is useful to, first, study the multiple amide unit excitations at a given chain configuration, i.e., the so-called adiabatic excitons (cf., e.g., Refs. 26 and 28). Adiabatic single-exciton states are obtained by diagonalizing $H_1 - T_{\mathrm{vib}} \hat{P}_1$ and two-exciton states by diagonalizing $H_2 - T_{\mathrm{vib}} \hat{P}_2$ [cf. Eqs. (17) and (18), respectively]. Their study is also justified by the fact that the upper limiting frequency for the chain motion is about one order of magnitude smaller than the basic frequency of amide vibrations.

In the subsequent section we further specify the used amide-unit chain model introduced in Sec. II and afterwards we present the results for the adiabatic exciton states. In any case, we shall study the chains of identical amide units, neglecting any effect of chain inhomogeneity and disorder (to stay at a uniform notation, this fact is not considered in the formulas).

A. Further specification of the model

As already indicated, our studies will focus on exclusive excitations of the amide unit C=O stretching mode which relevant parameters are well described in literature.[6,12] The anharmonicity of the C=O mode is accounted for by using a Morse potential for V_m and by adapting it to the amide I mode excitation energy of $E_1 - E_0 = 1660\ \mathrm{cm}^{-1}$,[15] as well as to the anharmonicity parameter $A = 10\ \mathrm{cm}^{-1}$ (see Appendix for more details). This parameter choice corresponds to that of Ref. 15, making our computations comparable with previous studies.

The nearest-neighbor coupling between the amide oscillators takes the form

$$V_{m,n}(Q_m, Q_n) = -\delta_{m+1,n} J Q_m Q_{m+1}, \tag{23}$$

with a coupling constant $J = 7.8\ \mathrm{cm}^{-1}$.[6] This formula corresponds to an approximation of a transition dipole moment coupling between different amide units with the dipole operators written as

$$\hat{\boldsymbol{\mu}}_m = \Delta \boldsymbol{\mu}_m Q_m. \tag{24}$$

The overall dipole operator which couples the amide vibrations to infrared photons simply follows as

$$\hat{\boldsymbol{\mu}} = \sum_m \hat{\boldsymbol{\mu}}_m. \tag{25}$$

When considering the chain vibrations it is sufficient to remain at a harmonic model with the standard potential

$$U(x) = \frac{W}{2} \sum_m (x_m - x_{m-1})^2. \tag{26}$$

The mass of amide unit amounts to 114 proton masses and the chain elastic force constant equals $W = 13\ \mathrm{N/m}$.[12]

The amide oscillator coupling to the chain coordinates is also written similar to Ref. 15 as

$$H_{\mathrm{coup}} = \frac{\chi}{2} \sum_{m>1} Q_m^2 (x_m - x_{m-1}). \tag{27}$$

The value of the coupling constant $\chi = 62$ pN is taken from Ref. 29.

The resulting matrix elements of the Hamiltonian entering Eqs. (17) and (18) are calculated in the Appendix. For the amide ground state potential energy surface (PES), i.e., for $H_0 - T_{\mathrm{vib}}$ [cf. Eq. (16)], we immediately obtain

$$\mathcal{E}_0(x) = \sum_m \left[(1 - \delta_{m,1}) \frac{W}{2} (x_m - x_{m-1})^2 + E_{m0} + w_{m0}(x) \right].$$

Besides the local amide oscillator ground-state energy E_{m0} [see Eq. (6)], this expression contains the functions $w_{m0}(x)$ following as the matrix elements of the coupling Hamiltonian, Eq. (27). The general type reads

$$w_{m\nu}(x) = (1 - \delta_{m,1}) \frac{\chi}{2} (x_m - x_{m-1}) \langle \chi_{m\nu} | Q_m^2 | \chi_{m\nu} \rangle. \tag{28}$$

Next, we turn to the single- and two-exciton states.

B. Adiabatic single-exciton states

To obtain the single adiabatic vibrational exciton states via diagonalizing $H_1 - T_{\mathrm{vib}} \hat{P}_1$, we take the ansatz

$$|\boldsymbol{\Phi}_\alpha(x)\rangle = \sum\nolimits_m C_\alpha(m;x) |\phi_m\rangle, \tag{29}$$

with normalization condition $\Sigma_m |C_\alpha(m;x)|^2 = 1$. The related eigenvalue equation for the single-exciton energies $\mathcal{E}_\alpha(x)$ reads

$$(H_1 - T_{\mathrm{vib}}) |\boldsymbol{\Phi}_\alpha(x)\rangle = \mathcal{E}_\alpha |\boldsymbol{\Phi}_\alpha(x)\rangle. \tag{30}$$

Note that the energies and expansion coefficients depend parametrically on the chain coordinates x. The matrix elements of the Hamiltonian H_1 with respect to singly excited states are given in the Appendix. Using Eq. (A9) we obtain

$$\begin{aligned} &(\mathcal{E}_0(x) + E_1 - E_0 + w_{m1}(x) - w_{m0}(x)) C_\alpha(m;x) \\ &\quad - (1 - \delta_{m,1}) J_1 C_\alpha(m-1;x) \\ &\quad - (1 - \delta_{m,N}) J_1 C_\alpha(m+1;x) = \mathcal{E}_\alpha C_\alpha(m;x), \end{aligned} \tag{31}$$

where J_1 stems from electrostatic interamide interactions and is given by Eq. (A10).

In order to elucidate the self-trapping effect of amide excitons, in a first step, we have performed a multidimensional minimization of the adiabatic exciton energy levels as

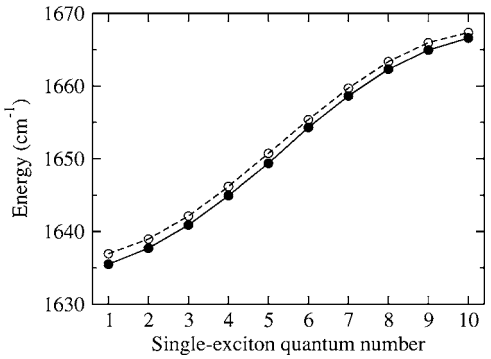

FIG. 1. Sequence of single-exciton energies for a chain of ten amide units vs exciton quantum number $\alpha=1,\ldots,10$ (all energies are defined with respect to the minimum of the ground-state PES). Open circles: values of $\mathcal{E}_\alpha(x)$ at the exciton ground-state chain equilibrium configuration x_0. Full circles: values following after relaxation into the configuration x_α corresponding to the minimum of $\mathcal{E}_\alpha(x)$ (the respective energetic differences define the reorganization energies λ_α).

functions of the chain coordinates. The obtained chain configurations are denoted by x_α, indicating that they are changing with changing exciton level. As a reference chain configuration x_0 we take that at the minimum of the exciton ground state PES $\mathcal{E}_0(x)$. Figure 1 shows the energy levels in the single-exciton manifold $\mathcal{E}_\alpha(x_0)$ at the reference chain configuration and the energy levels $\mathcal{E}_\alpha(x_\alpha)$ at the respective relaxed configuration. The difference $\mathcal{E}_\alpha(x_0)-\mathcal{E}_\alpha(x_\alpha)$ defines the relaxation (reorganization) energy, which is rather small and does not give any indication of single-exciton self-trapping. These results have to be distinguished from those of Ref. 25, where we used a symmetric form of the exciton-chain vibrational coupling Hamiltonian H_{coup} (it enforces the self-trapping effect).

To get an impression of the lowest single-exciton wave function ($\alpha=1$), the probability $|C_\alpha(m;x_\alpha)|^2$ to have a single excitation at amide unit m for this state is displayed in Fig. 2 (open circles). The form of the distribution remains unchanged if we increase the size of the chain. In Ref. 6 the width of the Davydov soliton was estimated as $14\ WJ/\chi^2$. For the parameters used here this estimate gives a width of approximately seven amide units, which agrees reasonably

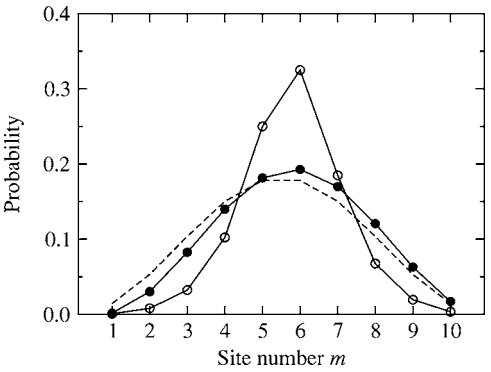

FIG. 2. Probability P_m to find a singly excited amide state at chain site m for the lowest single-exciton state $\alpha=1$ within different approximations. Open circles: probability distribution $|C_\alpha(m,x_\alpha)|^2$ of the adiabatic exciton. Full circles: probability $\int dx|\psi_m^{(\mathrm{rel})}(x)|^2$ determined from the fully relaxed exciton-chain vibrational wave function. Dashed line: $|C_\alpha(m)|^2$ of a rigid chain [neglect of H_{coup} in Eq. (1)].

with our numerical results. $\mathcal{E}_{\alpha=1}(x_{\alpha=1})$ represents the global minimum of the single-exciton energy levels. Higher-lying local minima of $\mathcal{E}_{\alpha=1}$ correspond to the shift of the excitonic wave function more to one of the chain ends, but they are energetically nearly degenerated with the global minimum. In the full quantum description taking into account the motion of the chain units, different self-trapped states form a common superposition state. Respective calculations of the full exciton-chain vibrational wave function will be described in Sec. IV B.

C. The two-exciton states

The determination of adiabatic vibrational two-exciton states is similar to that of single-exciton states as demonstrated in the preceding section. They are introduced via diagonalizing $H_1-T_{\mathrm{vib}}\hat{P}_2$ using the ansatz

$$|\tilde{\mathbf{\Phi}}_{\tilde{\alpha}}(x)\rangle=\sum\nolimits_{m\leqslant n}C_{\tilde{\alpha}}(m,n;x)|\tilde{\phi}_{m,n}\rangle \tag{32}$$

with normalization condition $\Sigma_{m\leqslant n}|C_{\tilde{\alpha}}(m,n;x)|^2=1$. The two-exciton eigenvalue equation fixing the two-exciton energies $\mathcal{E}_{\tilde{\alpha}}(x)$ reads as follows:

$$(H_2-T_{\mathrm{vib}})|\tilde{\mathbf{\Phi}}_{\tilde{\alpha}}(x)\rangle=\mathcal{E}_{\tilde{\alpha}}|\tilde{\mathbf{\Phi}}_{\tilde{\alpha}}(x)\rangle. \tag{33}$$

Noting the Eqs. (A11) and (A12) for the matrix elements of H_2, it leads to $(m=n)$

$$\begin{aligned}&(\mathcal{E}_0(x)+E_2-E_0+w_{m2}(x)-w_{m0}(x))C_{\tilde{\alpha}}(m,m;x)\\&\quad-(1-\delta_{m,1})J_2C_{\tilde{\alpha}}(m-1,m;x)-(1-\delta_{m,N})\\&\quad\times J_2C_{\tilde{\alpha}}(m,m+1;x)=\mathcal{E}_{\tilde{\alpha}}C_{\tilde{\alpha}}(m,m;x),\end{aligned} \tag{34}$$

with J_2 introduced in Eq. (A12). In the case of $m\neq n$ we obtain

$$\begin{aligned}&(\mathcal{E}_0(x)+2E_1-2E_0+w_{m1}(x)-w_{m0}(x)+w_{n1}(x)\\&\quad-w_{n0}(x))C_{\tilde{\alpha}}(m,n;x)-\delta_{m,n-1}J_2C_{\tilde{\alpha}}(m,m;x)\\&\quad-\delta_{m,n-1}J_2C_{\tilde{\alpha}}(n,n;x)-\sum_k((\delta_{k,m-1}+\delta_{k,m+1})\\&\quad\times(1-\delta_{k,n})J_1C_{\tilde{\alpha}}(k,n;x)+(\delta_{k,n-1}+\delta_{k,n+1})\\&\quad\times(1-\delta_{k,m})J_1C_{\tilde{\alpha}}(m,k;x))=\mathcal{E}_{\tilde{\alpha}}C_{\tilde{\alpha}}(m,n;x),\quad m\neq n.\end{aligned} \tag{35}$$

Results of the energy level minimization for the two-exciton manifold are shown in Fig. 3. As in the single-exciton case, energies for the exciton ground-state chain equilibrium configuration x_0 and for relaxed configurations $x_{\tilde{\alpha}}$ are presented. The reorganization energy $\mathcal{E}_{\tilde{\alpha}}(x_0)-\mathcal{E}_{\tilde{\alpha}}(x_{\tilde{\alpha}})$ for the two states at the lower edge of the two-exciton level manifold is significantly larger than the respective energies for higher-lying levels. This has to be considered as a pronounced indication of two-exciton self-trapping as also obtained in Refs. 15–17.

To analyze the details of these self-trapped states the respective on-site probability distribution $|C_{\tilde{\alpha}}(m,m;x_{\tilde{\alpha}})|^2$ for the lowest adiabatic two-exciton state ($\tilde{\alpha}=1$) is shown in Fig. 4 (open circles). It is essentially localized on one chain unit (compare with Ref. 15). The two-exciton level $\tilde{\alpha}=2$ results

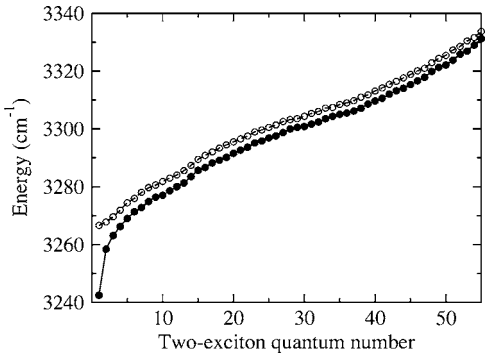

FIG. 3. Sequence of two-exciton energies for a chain of ten amide units vs two-exciton quantum number $\tilde{\alpha}=1,\ldots,55$ (all energies are defined with respect to the minimum of the ground-state PES). Open circles: values of $\mathcal{E}_{\tilde{\alpha}}(x)$ at the exciton ground-state chain equilibrium configuration x_0. Full circles: values following after relaxation into the configuration $x_{\tilde{\alpha}}$ corresponding to the minimum of $\mathcal{E}_{\tilde{\alpha}}(x)$ (the respective energetic differences define the reorganization energies $\lambda_{\tilde{\alpha}}$).

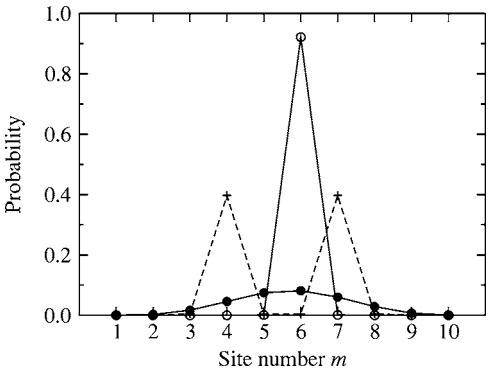

FIG. 4. Probability P_{mm} to find a doubly excited amide state at chain site m for the lowest two-exciton state $\tilde{\alpha}=1$ within different approximations. Open circles: probability distribution $|C_{\tilde{\alpha}}(m,m;x_{\tilde{\alpha}})|^2$ of the adiabatic two-exciton state. Full circles: probability $\int dx|\tilde{\psi}^{(\mathrm{rel})}_{m,m}(x)|^2$ determined from the fully relaxed exciton-chain vibrational wave function. [The dashed line shows the probability distribution $|C_{\tilde{\alpha}}(m,m;x_{\tilde{\alpha}})|^2$ for the higher-lying adiabatic two-exciton state $\tilde{\alpha}=2$.]

in a second type of self-trapped state (crosses in Fig. 4). This state describes the self-trapping of double on-site excitation at two different units of the chain (cf. also Ref. 15). The excited units are separated by two chain sites from each other, whereas in Ref. 15 self-trapping on the nearest-neighbor units was reported. This difference appears since the amide mode coupling to the chain deformations as assumed in Ref. 15 has a symmetric form, which depends on the displacements of two nearest neighbors of the given chain unit. However, it was suggested[6] that the asymmetric form of the coupling, cf. Eq. (27), is more appropriate in describing the real situation in an α-helix, where the C═O stretching mode interacts primarily with one adjacent hydrogen bond. Within our calculations the result of Ref. 15 is revealed if we use the symmetric form of the coupling in Eq. (27). Energy minimization for adiabatic two-exciton states with $\tilde{\alpha}>2$ results in essentially delocalized wave functions.

Although the presented data for adiabatic two-exciton states offer an interesting insight into the structure of the self-trapped state, this approach remains incomplete. Considering a longer chain than that of the ten units analyzed here one expects that the lowest self-trapped two-exciton state will again be formed in the center of the chain. However, there are similar self-trapped states in the neighborhood only slightly above in energy with respect to the lowest state. If the effect of the chain ends is further diminished by increasing the chain length, all these states start to degenerate indicating that the use of adiabatic two-exciton (as well as single-exciton) levels would be inappropriate when studying, for example, optical transition among the manifolds. Now, a superposition of all these quasidegenerated states has to be considered. This is just achieved in a full quantum description of the exciton-chain dynamics.

IV. VIBRATIONAL WAVE PACKET DYNAMICS

The adiabatic exciton states, Eqs. (29) and (32), provide a direct tool to characterize the exciton self-trapping effect (cf. Ref. 25). Possible degeneracy and superposition of these states, however, has to be accounted for by the construction of the complete exciton-chain vibrational wave function. The stationary lowest single- and two-exciton states can be studied using wave function relaxation within the MCTDH approach. In the following, the application of the MCTDH method for exciton-chain vibrational wave packet propagation and relaxation will be described, with the final aim to calculate the linear and transient infrared absorption spectra.

The computation of the complete exciton-chain vibrational wave function can be achieved by using a representation with respect to the adiabatic exciton states. However, since they are all related one to another by nonadiabatic couplings, it is rather advisable to use the basis of local multiexcited amide states, Eqs. (8)–(11). Restricting again our consideration to the amide ground state, as well as the manifolds of singly and doubly excited states, the expansion of an arbitrary state vector reads

$$|\Psi(t)\rangle = \psi_0(x,t)|0\rangle + \sum_m \psi_m(x,t)|\phi_m\rangle + \sum_{m\leqslant n} \tilde{\psi}_{m,n}(x,t)|\tilde{\phi}_{m,n}\rangle. \tag{36}$$

The expansion coefficients $\psi_0(x,t)$, $\psi_m(x,t)$, and $\tilde{\psi}_{m,n}(x,t)$ have to be understood as vibrational wave functions of the (remaining) chain coordinates x. Inserting the expansion (36) into the time-dependent Schrödinger equation we get

$$i\hbar\frac{\partial}{\partial t}\psi_0(x,t) = \langle 0|H_{\mathrm{mol}}|0\rangle\psi_0(x,t), \tag{37}$$

$$i\hbar\frac{\partial}{\partial t}\psi_m(x,t) = \sum_n \langle\phi_m|H_{\mathrm{mol}}|\phi_n\rangle\psi_n(x,t), \tag{38}$$

$$i\hbar\frac{\partial}{\partial t}\tilde{\psi}_{m,n}(x,t) = \sum_{k\leqslant l} \langle\tilde{\phi}_{m,n}|H_{\mathrm{mol}}|\tilde{\phi}_{k,l}\rangle\tilde{\psi}_{k,l}(x,t). \tag{39}$$

Note that matrix elements of the Hamiltonian describing the coupling between different manifolds of excited states are not included into Eqs. (37)–(39). This allows one to solve each set of equations independently and also to perform relaxation of the wave function within the zero-exciton, single-

exciton, and two-exciton manifolds. However, in Sec. V (full-dimensional) MCTDH calculations will be carried out which do not rely on the multiexciton expansion and implicitly take into account all matrix elements of the Hamiltonian. These calculations will be used to estimate the effect of intermanifold couplings on the resulting infrared absorption spectra.

A. Wave packet propagation within the MCTDH approach

Applying the MCTDH approach,[24] the multitude of chain vibrational wave functions $\psi_0(x,t)$, $\psi_m(x,t)$, and $\tilde{\psi}_{m,n}(x,t)$ is represented as a time-dependent superposition of Hartree products of time-dependent single chain coordinate wave functions (so-called single particle functions).

Starting with the chain vibrational wave function for the amide excitation ground state, the representation appropriate for the MCTDH method is rather standard. Noting the change to new chain coordinates

$$y_\kappa = x_{\kappa+1} - x_\kappa, \quad \kappa = 1, \ldots, N-1, \tag{40}$$

we have to set

$$\psi_0(y,t) = \sum_{j_1=1}^{M_1} \sum_{j_2=1}^{M_2} \cdots \sum_{j_{N-1}}^{M_{N-1}} A^{(0)}_{j_1 j_2 \cdots j_{N-1}}(t) \prod_{\kappa=1}^{N-1} \varphi^{(0)}_{j_\kappa}(y_\kappa,t). \tag{41}$$

Here M_κ is the number of single particle functions $\varphi^{(0)}_{j_\kappa}(y_\kappa,t)$ for mode κ and the $A^{(0)}_{j_1 j_2 \cdots j_{N-1}}(t)$ are the expansion coefficients for the particular Hartree products $\Pi_\kappa \varphi^{(0)}_{j_\kappa}(y_\kappa,t)$.

When choosing the representation of the vibrational wave functions belonging to the singly and doubly excited states we have to note that within a given manifold they are all coupled (which is similar to the description of nonadiabatic transitions in standard MCTDH applications). In the two-exciton case we have to account for 55 different states. Accordingly, the representation of the singly and doubly excited state wave functions are as follows:

$$\psi_m(y,t) = \sum_{j_1=1}^{M_1} \sum_{j_2=1}^{M_2} \cdots \sum_{j_{N-1}}^{M_{N-1}} A^{(m)}_{j_1 j_2 \cdots j_{N-1}}(t) \prod_{\kappa=1}^{N-1} \varphi^{(m)}_{j_\kappa}(y_\kappa,t) \tag{42}$$

and

$$\tilde{\psi}_{m,n}(y,t) = \sum_{j_1=1}^{M_1} \sum_{j_2=1}^{M_2} \cdots \sum_{j_{N-1}}^{M_{N-1}} A^{(m,n)}_{j_1 j_2 \cdots j_{N-1}}(t) \prod_{\kappa=1}^{N-1} \varphi^{(m,n)}_{j_\kappa}(y_\kappa,t), \tag{43}$$

respectively.

Equations of motion for the single-particle functions φ and the expansion coefficients can be formulated based on the Dirac-Frenkel variational principle $\langle \delta\Psi(t) | i\hbar\partial/\partial t - H_{\mathrm{mol}} | \Psi(t)\rangle = 0$ (see Ref. 24). The respective equations are the basis of the *Heidelberg* MCTDH *program package*,[30] which has been applied for the numerical calculations presented below. The computations are based on the constant mean field (CMF) integration scheme. For the time-propagation of the expansion coefficients A the short iterative Lanczos (SIL) integrator is used. Propagation of the single-particle functions φ is performed using the Bulirsch-Stoer (BS) integrator (see Ref. 30 and references therein). The relaxed wave functions $\psi_0^{(\mathrm{rel})}(x)$ and $\psi_m^{(\mathrm{rel})}(x)$, and $\tilde{\psi}_{mn}^{(\mathrm{rel})}(x)$ corresponding to the zero-exciton, single-exciton, and two-exciton manifold ground states, respectively, are obtained using the imaginary time propagation part of the program package. Table I summarizes the simulation parameters.

TABLE I. Parameters used in the MCTDH program package for the calculations within the multiexciton model (MEM, cf. Sec. IV) and for the full-dimensional calculations (FDC, cf. Sec. V). N and M_κ are parameters of the MCTDH wave function representation, Eqs. (41)–(43). The typical numerical effort for the propagation of the exciton-chain vibrational wave function is estimated from the usage of computer memory (RAM) and CPU time. The full-dimensional calculations were performed for the chain length of five amide units, whereas in the case of the multiexciton model the chain length is ten amide units. The calculations were performed on the 1.67 GHz AMD Athlon processor. See text for the explanation of the integrator names.

Parameters	MEM	FDC
Representation of the wave function		
N	10	5
M_κ ($\kappa=1,\ldots,N-1$)	3	4
Primitive basis size	30	60
The CMF integration scheme		
Initial step size (fs)	0.5	0.5
Error tolerance	10^{-6}	10^{-6}
The SIL integrator		
Integration order	15	15
Error tolerance	10^{-7}	10^{-7}
The BS integrator		
Integration order	9	9
Error tolerance	10^{-7}	10^{-7}
Single-exciton wave function propagation		
Usage of RAM (MB)	65	90
CPU time per fs (s)	1.9	8.5

B. Results for wave packet relaxation

First, the MCTDH method is applied for an imaginary time propagation[24,30] in the zero-exciton state and in the manifolds of singly and doubly excited amide states. This procedure results in the (numerically) exact relaxed zero-exciton wave function $|\Psi_0^{(\mathrm{rel})}\rangle = \psi_0^{(\mathrm{rel})}(x)|0\rangle$, as well as the relaxed single- and two-exciton wave functions. The relaxed single-exciton wave function reads

$$|\Psi_1^{(\mathrm{rel})}\rangle = \sum_m \psi_m^{(\mathrm{rel})}(x)|\phi_m\rangle. \tag{44}$$

For the two-exciton manifold we obtain the relaxed chain vibrational wave function as

$$|\Psi_2^{(\mathrm{rel})}\rangle = \sum_{m \le n} \tilde{\psi}_{mn}^{(\mathrm{rel})}(x)|\tilde{\phi}_{mn}\rangle. \tag{45}$$

To characterize the single-exciton chain vibrational ground state the probability distribution $P_m = \int dx |\psi_m^{(\mathrm{rel})}(x)|^2$ is shown

in Fig. 2 (full circles). As expected, this distribution is broader than that for the adiabatic exciton. The absence of notable single-exciton self-trapping lets P_m almost coincide with the distribution $[2/(N+1)]\sin^2(\pi m/(N+1))$ for a rigid chain (dashed line).

The two-exciton chain vibrational ground state is analyzed by computing the probability distribution $P_{mm}=\int dx|\tilde{\psi}^{(\mathrm{rel})}_{mm}(x)|^2$, cf. Fig. 4 (full circles). This distribution results from the quantum superposition of self-trapped states positioned at different parts of the chain and corresponding to the double on-site excitations of the amide units. Therefore, P_{mm} is broadened compared to the adiabatic exciton result (open circles). It is important to mention that the probabilities P_{mm} represent only the diagonal part of the full two-exciton ground-state probability distribution $P_{mn}=\int dx|\tilde{\psi}^{(\mathrm{rel})}_{mn}(x)|^2$.

V. THE SEQUENTIAL TRANSIENT ABSORPTION SPECTRUM

Motivated by the experiments reported in Ref. 7 and respective simulations in Ref. 17 we compute the infrared transient absorption spectra (TAS) in the following. In order to do this one has different options. On the one hand side, there is the well-established approach based on the third-order nonlinear response function of the molecular system.[31] Since this quantity depends on three independent time arguments its complete computation is possible for simple systems where the nonlinear reponse can be calculated analytically. The method, however, is less suitable for systems in which the dynamics can only be aquired numerically as in the present case.

This difficulty is overcome by the other approach based on the solution of the time-dependent Schrödinger equation in the *presence* of the pump and probe fields. Once this has been done the TAS can be calculated by a proper analysis of the overall polarization and a selection of the probe-pulse induced component as suggested in Ref. 32. The method would be also adequate to the present case; however, we choose a technique to get the TAS which is adopted to the sequential character of the related pump-probe experiment.

We also account for the action of the pump field in a nonperturbative manner, but an expansion with respect to the probe pulse field strength is carried out, which is of first order only. Then, the related linear response function is calculated at times after the pump-pulse action where the system stays in an excited but stationary state. The subsequent computation is based on the time propagation of respective wave functions and a Fourier transformation of the related correlation function as it is rather standard when determining the linear absorption spectra (see, for example, Ref. 26). Since this approach is new when used to calculate the TAS, we shortly explain its main steps.

Within a pump-probe scheme we set for the overall field

$$\mathbf{E}(\mathbf{r},t)=\mathbf{E}_{\mathrm{pu}}(\mathbf{r},t)+\mathbf{E}_{\mathrm{pr}}(\mathbf{r},t) \equiv \sum_{p=\mathrm{pu,pr}} \mathbf{e}_p E_p(t)\exp(i(\mathbf{k}_p\mathbf{r}-\omega_p t))+\mathrm{c.c.}. \tag{46}$$

The polarization unit vectors and pulse envelopes are given by $\mathbf{e}_p$ and $E_p(t)$, respectively, the $\mathbf{k}_p$ are wave vectors, and the ω_p denote the carrier frequencies. The total polarization (at the absence of inhomogeneous broadening) is obtained from the expectation value of the dipole operator

$$\mathbf{P}(\mathbf{r},t)=n_{\mathrm{mol}}\,\mathrm{tr}\{\hat{\boldsymbol{\mu}}\hat{W}(t;\mathbf{E})\}, \tag{47}$$

where $\hat{W}$ denotes the statistical operator of the system and n_{mol} is the volume density of the considered molecules. For the polarization field induced by the probe pulse we expect the following form:

$$\mathbf{P}_{\mathrm{pr}}(\mathbf{r},t)=\mathbf{e}_{\mathrm{pr}}P_{\mathrm{pr}}(t)\exp(i(\mathbf{k}_{\mathrm{pr}}\mathbf{r}-\omega_{\mathrm{pr}}t))+\mathrm{c.c.}, \tag{48}$$

which has to be deduced from the overall polarization.

The probe-pulse TAS, then, takes the following form:

$$S_{\mathrm{pr}}(t)=-\int d^3\mathbf{r}\frac{\partial\mathbf{E}_{\mathrm{pr}}(t)}{\partial t}\mathbf{P}_{\mathrm{pr}}(t)\approx 2V\omega_{\mathrm{pr}}\,\mathrm{Im}[E^*_{\mathrm{pr}}(t)P_{\mathrm{pr}}(t)]. \tag{49}$$

This expression gives the energy gain per time that the molecular system experiences at the presence of the probe field (V denotes the sample volume). The total energy gain is as follows:

$$S^{(\mathrm{tot})}_{\mathrm{pr}}=\int dt S_{\mathrm{pr}}(t)=\int d\omega S_{\mathrm{pr}}(\omega), \tag{50}$$

with the frequency dispersed TAS

$$S_{\mathrm{pr}}(\omega)=\frac{\omega_{\mathrm{pr}}V}{\pi}\,\mathrm{Im}[E^*_{\mathrm{pr}}(\omega)P_{\mathrm{pr}}(\omega)]. \tag{51}$$

Usually, the probe pulse is weak and we may determine P_{pr} linear in the probe field (but it remains a nonlinear functional with respect to the pump field). The respective relation between the field envelopes reads

$$P_{\mathrm{pr}}(t)=\int d\bar{t}e^{i\omega_{\mathrm{pr}}(t-\bar{t})}R_{\mathrm{pr}}(t,\bar{t})E_{\mathrm{pr}}(\bar{t}), \tag{52}$$

where the probe-pulse response function can be deduced from Eq. (47) after linearizing the statistical operator $\hat{W}(t)$ with respect to the probe field. Using $\hat{\mu}=\mathbf{e}_{\mathrm{pr}}\hat{\boldsymbol{\mu}}$ we get

$$R_{\mathrm{pr}}(t,\bar{t})=\frac{i}{\hbar}\Theta(t-\bar{t})\mathrm{tr}\{\hat{\mu}U(t,\bar{t};\mathbf{E}_{\mathrm{pu}}) \times[\hat{\mu},\hat{W}(\bar{t};\mathbf{E}_{\mathrm{pu}})]_- U^+(t,\bar{t};\mathbf{E}_{\mathrm{pu}})\}. \tag{53}$$

In the following we exclusively consider a sequential pump-probe experiment, i.e., we will deal with a situation where the pump and the probe-pulse do not overlap in time. Then, according to the time integration in Eq. (52) which includes $E_{\mathrm{pr}}(\bar{t})$, only those $\bar{t}$-values at which the pump field already vanished have to be considered. This enables us to replace the time evolution operator $U(t,\bar{t};\mathbf{E}_{\mathrm{pu}})$ by that of the isolated molecule at the absence of any external field, denoted as U_{mol}. Moreover, we assume that at the presence of the probe field the molecule has already relaxed into a quasi-stationary state characterized by the statistical operator $\hat{W}_{\mathrm{rel}}$. This all results in

$$R_{\mathrm{pr}}(t-\bar{t}) = \frac{i}{\hbar}\Theta(t-\bar{t})\mathrm{tr}\{\hat{\mu}U_{\mathrm{mol}}(t-\bar{t})[\hat{\mu},\hat{W}_{\mathrm{rel}}]_{-}U^{+}_{\mathrm{mol}}(t-\bar{t})\}. \tag{54}$$

Since R_{pr} now depends on the time difference, the Fourier-transformed probe polarization takes the form

$$P_{\mathrm{pr}}(\omega) = R_{\mathrm{pr}}(\omega+\omega_{\mathrm{pr}})E_{\mathrm{pr}}(\omega), \tag{55}$$

and the frequency dispersed TAS follows as:

$$S_{\mathrm{pr}}(\omega) = \frac{\omega_{\mathrm{pr}}V}{\pi}|E_{\mathrm{pr}}(\omega)|^2\ \mathrm{Im}\ R_{\mathrm{pr}}(\omega+\omega_{\mathrm{pr}}). \tag{56}$$

In order to compute this expression we have to specify the relaxed state after pump-pulse action. It is assumed as a mixed state of a depleted ground state and some excitation in the single-exciton manifold

$$\hat{W}_{\mathrm{rel}} = w_0|\Psi_0^{(\mathrm{rel})}\rangle\langle\Psi_0^{(\mathrm{rel})}| + w_1|\Psi_1^{(\mathrm{rel})}\rangle\langle\Psi_1^{(\mathrm{rel})}|. \tag{57}$$

A population of higher manifolds is neglected, thus, assuming not too strong excitation by the pump pulse. w_0 and w_1 denote the overall populations of the ground state and of the manifold of singly excited states, respectively $(w_0+w_1=1)$. In order to calculate the response function R_{pr}, Eq. (54), we introduce $\hbar\Omega_0^{(\mathrm{rel})}$ and $\hbar\Omega_1^{(\mathrm{rel})}$ as the energies of both relaxed states (lowest eigenvalue of H_0 and H_1, respectively) and use Eq. (57), and obtain:

$$\begin{aligned} R_{\mathrm{pr}}(\tau) = \frac{i}{\hbar}\Theta(\tau) \times (& w_0 e^{i\Omega_0^{(\mathrm{rel})}\tau}\langle\Psi_0^{(\mathrm{rel})}|\hat{\mu}_{01}e^{-iH_1\tau/\hbar}\hat{\mu}_{10}|\Psi_0^{(\mathrm{rel})}\rangle \\ &+ w_1 e^{i\Omega_1^{(\mathrm{rel})}\tau}\langle\Psi_1^{(\mathrm{rel})}|[\hat{\mu}_{10}e^{-iH_0\tau/\hbar}\hat{\mu}_{01} \\ &+ \hat{\mu}_{12}e^{-iH_2\tau/\hbar}\hat{\mu}_{21}]|\Psi_1^{(\mathrm{rel})}\rangle) + \mathrm{c.c.} \end{aligned} \tag{58}$$

Note the ordering of the dipole operator with respect to the different manifolds (for example, $\hat{\mu}_{12}=\hat{P}_1\hat{\mu}\hat{P}_2$).

The contribution proportional to w_0 describes the absorption from the ground state via time propagation of $\hat{\mu}_{10}|\Psi_0^{(\mathrm{rel})}\rangle$ within the single-exciton manifold followed by an overlap with its initial value. In the same manner the second term in Eq. (58) gives the stimulated emission contribution via propagation of $\hat{\mu}_{01}|\Psi_1^{(\mathrm{rel})}\rangle$ in the ground state. Excited state absorption into the two-exciton manifold follows by propagating $\hat{\mu}_{21}|\Psi_1^{(\mathrm{rel})}\rangle$ in the space of double excitations. All mentioned propagations are carried out as described in Sec. IV, i.e., by using an expansion in locally excited states.

Usually, the differential TAS is represented as

$$\begin{aligned} \Delta S_{\mathrm{pr}}(\omega) &= S_{\mathrm{pr}}(\omega;\mathbf{E}_{\mathrm{pu}}\neq 0) - S_{\mathrm{pr}}(\omega;\mathbf{E}_{\mathrm{pu}}=0) \\ &= \frac{\omega_{\mathrm{pr}}V}{\pi}|E_{\mathrm{pr}}(\omega)|^2\ \mathrm{Im}[R_{\mathrm{pr}}^{(\mathrm{GB})}(\omega+\omega_{\mathrm{pr}}) \\ &\quad + R_{\mathrm{pr}}^{(\mathrm{EA})}(\omega+\omega_{\mathrm{pr}}) + R_{\mathrm{pr}}^{(\mathrm{SE})}(\omega+\omega_{\mathrm{pr}})]. \end{aligned} \tag{59}$$

Note the indication whether or not the pump pulse has been applied. The three components of the differential TAS in Eq. (59) correspond to the ground-state bleaching (GB), stimulated emission (SE), and excited-state absorption (EA) processes. Their explicit expressions follow from Eq. (58) (so-called antiresonant contributions have been neglected):

$$R_{\mathrm{pr}}^{(\mathrm{GB})}(\omega) = -\frac{i}{\hbar}w_1\int_0^\infty d\tau e^{i(\omega+\Omega_{\mathrm{rel}}^{(0)})\tau} \times\sum_m \int dx d_1^*\psi_0^{(\mathrm{rel})*}(x)\psi_m(x,\tau), \tag{60}$$

$$R_{\mathrm{pr}}^{(\mathrm{SE})}(\omega) = -\frac{i}{\hbar}w_1\int_0^\infty d\tau e^{i(\omega-\Omega_{\mathrm{rel}}^{(1)})\tau} \times\sum_m \int dx d_1^*\psi_m^{(\mathrm{rel})}(x)\psi_0^*(x,\tau), \tag{61}$$

and

$$\begin{aligned} R_{\mathrm{pr}}^{(\mathrm{EA})}(\omega) = \frac{i}{\hbar}w_1\int_0^\infty d\tau e^{i(\omega+\Omega_{\mathrm{rel}}^{(1)})\tau} &\times \sum_{m\leqslant n}\int dx\Big[\delta_{m,n}d_2^*\psi_m^{(\mathrm{rel})*}(x)\tilde{\psi}_{mm}(x,\tau) \\ &+ [1-\delta_{m,n}]d_1^*(\psi_m^{(\mathrm{rel})*}(x)+\psi_n^{(\mathrm{rel})*}(x))\tilde{\psi}_{mn}(x,\tau)\Big], \end{aligned} \tag{62}$$

where $d_1=(\mathbf{e}_{\mathrm{pr}}\mathbf{d}_1)$ and $d_2=(\mathbf{e}_{\mathrm{pr}}\mathbf{d}_2)$ denote projections of the local transition dipole moments, Eqs. (A18) and (A19), on the probe-field polarization direction. Within the numerical calculations an overall dephasing is introduced via multiplying the expressions under the time integral with $\exp(-\tau/\tau_{\mathrm{deph}})$. In the following, the probe-field polarization direction $\mathbf{e}_{\mathrm{pr}}$, as well as the transition dipole moments $\mathbf{d}_1$ and $\mathbf{d}_2$, will be chosen parallel to the axis of the peptide chain, which we consider as a reasonable one-dimensional description of the α-helical structure (note that the direction of the transition dipole moments in polypeptides in the three-dimensional case can be found in Ref. 33).

The spectrum of linear absorption can be deduced from $R_{\mathrm{pr}}^{(\mathrm{GB})}(\omega)$, Eq. (60) at $w_1=-1$, i.e., we obtain the standard relation

$$\begin{aligned} S_{\mathrm{pr}}(\omega;\mathbf{E}_{\mathrm{pu}}=0) &= \frac{\omega_{\mathrm{pr}}V}{\pi\hbar}|E_{\mathrm{pr}}(\omega)|^2\ \mathrm{Re}\int_0^\infty d\tau e^{i(\omega+\omega_{\mathrm{pr}}+\Omega_{\mathrm{rel}}^{(0)}+i/\tau_{\mathrm{deph}})\tau} \\ &\quad\times\sum_m\int dx d_1^*\psi_0^{(\mathrm{rel})*}(x)\psi_m(x,\tau). \end{aligned} \tag{63}$$

The spectrum is essentially given by the Fourier transform of the autocorrelation function multiplied by the spectral density of the probe pulse.

A. Results for the linear absorption

In a first step, we compare the results obtained in using the multiexciton expansion of the Hamiltonian, with the calculations explicitly taking into account the wave function dependence on the amide coordinates Q (full-dimensional calculations). Since the dimensionality of such calculations is two times larger than for the case of the multiexciton expansion, the numerical effort is significantly increased. For example, time propagation of the single-exciton wavefunc-

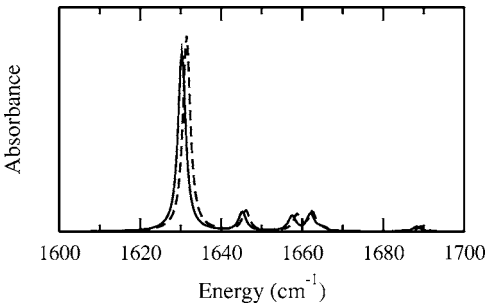

FIG. 5. Test calculations for the linear absorption spectrum of a chain with five amide units. The full and dashed lines show the results of full-dimensional calculations and the multiexciton model, respectively. For this and other presented plots of absorption spectra the energy scale is $\hbar(\omega+\omega_{pr})$ and the broadening of the spectral lines corresponds to the dephasing time $\tau_{deph}=5$ ps.

tion has approximately the same numerical requirements as the time propagation of the full-dimensional wave function for a two times smaller chain length (cf. Table I). Figure 5 offers a comparison of the linear absorption spectra obtained within the multiexciton model and using the full-dimensional calculations. The tests were performed for a chain of five amide units (cf. Fig. 5) and for chains of three and four amide units (data not shown). The small energy shift of the main absorption peak appears since the intermanifold coupling matrix elements of the Hamiltonian, Eqs. (A13)–(A15), are not included in the multiexciton model calculations. In the full-dimensional case, however, coupling between different excited states is implicitly taken into account.

Coupling to the higher excited states is primarily introduced by the term H_{coup} of the Hamiltonian [cf. Eq. (4)]. By varying the corresponding coupling constant χ one can estimate the behavior of the energy shift resulting from the multiexciton expansion of the Hamiltonian. Figure 6 shows the results obtained for a chain of three amide units and for

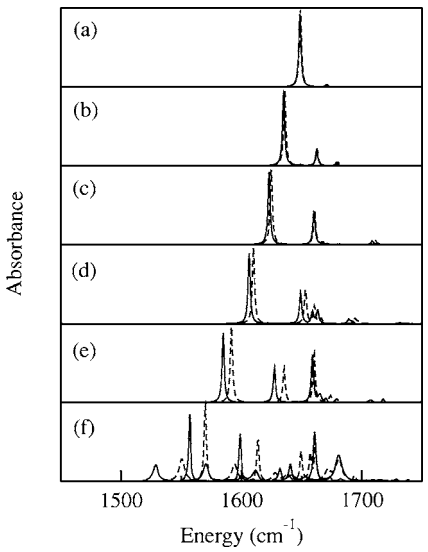

FIG. 6. Test calculations for the linear absorption spectra of a chain with three amide units and for different values of the exciton-chain vibrational coupling constant χ. The full lines show the results of full-dimensional MCTDH calculations, and the dashed lines correspond to the results of the respective exciton model. Calculations were done for χ values: (a) 0 pN, (b) 60 pN, (c) 80 pN, (d) 100 pN, (e) 120 pN, and (f) 140 pN.

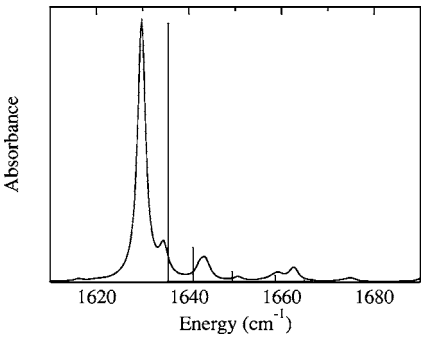

FIG. 7. Linear absorption spectrum for a chain of ten amide units. The vertical lines indicate the energetic position and oscillator strength of the adiabatic exciton states.

different values of the constant χ ranging from 0 to 140 pN. For $\chi=0$ pN there is only a negligible energy shift introduced by the potential terms $V_{m,n}(Q_m,Q_n)$, Eq. (23). With an increasing value of χ the linear absorption spectra obtained using the multiexciton expansion of the Hamiltonian start to deviate from the results of the full-dimensional calculations. It is necessary to note that for the χ value as large as 180 pN the coupling term H_{coup} significantly modifies the full energy spectrum, so that no bound single-exciton states exist for the system Hamiltonian, Eq. (1).

Having performed the accuracy tests, the linear infrared absorption spectrum has been calculated for a chain of ten amide units using the MCTDH approach (see Fig. 7). To understand the structure of the spectrum it is compared with the stick spectrum corresponding to the adiabatic excitons with the respective oscillator strength according to $|\Sigma_m C_\alpha(m;x_\alpha)|^2$ (cf. Sec. III). The maximum of the spectrum corresponds to the energy of the lowest single-exciton state. This energy is 5.5 cm^{-1} lower than in the adiabatic case. The energy difference demonstrates the importance of nonadiabatic effects in the motion of chain coordinates.

Since there does not exist a unique parameter χ of the exciton-chain vibrational coupling,[6] we have performed a series of calculations for different values of this parameter. The results for a chain of ten amide units are displayed in Fig. 8 ($\chi=0-120$ pN). With increasing χ the peak corresponding to the lowest exciton level shifts to lower frequencies. The sequence of spectral lines appearing on the high-energy side represents the progression of chain-vibrational levels separated by the energy quantum of 13 cm^{-1}, which can be identified as the chain vibration with the lowest frequency. However, the whole absorption spectrum is originated by a superposition of exciton-chain vibrational states, involving $N-1$ low-frequency normal-mode vibrations of the chain.

B. Results for the transient absorption

The three components of the pump-probe spectrum of the C=O stretching mode—the ground state bleaching, the stimulated emission, and the excited-state absorption spectrum-calculated according to the Eqs. (60)–(62) are plotted in Fig. 9(a). The maximum corresonding to excited-state

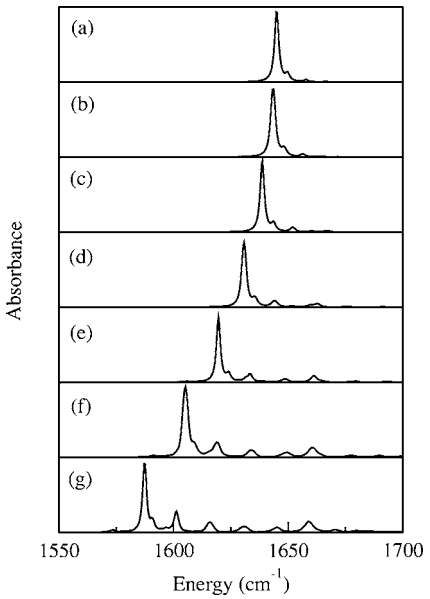

FIG. 8. Linear absorption spectrum (same as in the Fig. 7) for different values of the exciton-chain vibrational coupling constant χ: (a) χ=0 pN, (b) χ=20 pN, (c) χ=40 pN, (d) χ=60 pN, (e) χ=80 pN, (f) χ=100 pN, and (g) χ=120 pN.

absorption is shifted to lower frequencies with respect to the minimum originating from stimulated emission and ground-state bleaching processes what is a consequence of the amide mode anharmonicity. The full pump-probe spectrum following as a sum of the three signals, Eq. (59), is shown in Fig. 9(b). Its positive band is formed due to transitions from the lowest single-exciton state into self-trapped two-exciton states. As was pointed out in Ref. 34, the two-exciton states undergo relaxation on a time scale of 0.1–1 ps. Here, we use the line broadening corresponding to a lifetime of 5 ps in order to demonstrate the details of the spectrum. The TAS has also been presented in Ref. 17, but only concentrating on the single- and two-exciton levels without taking account of the chain vibrations. According to our knowledge, the present calculations of the sequential TAS are the first which are based on a numerically exact full quantum description of the exciton-chain vibrational dynamics.

C. Comparison with the experiment

Numerous experimental studies of linear and pump-probe absorption spectra have been carried out for polypeptide model systems, e.g., acetanilide, forming molecular crystals with hydrogen bonding (see, e.g., Ref. 8). In the case of the amide I band and at low temperatures the main linear absorption peak is believed to be originated from the self-trapped amide state [which is accompanied by a less pronounced phonon progression at its high-energy side, cf. Fig. 3(a) of Ref. 8]. This observation is in qualitative agreement with our results, Fig. 7, which, however, have been obtained for typical parameters of an α-helical polypeptide.[6,15] Since the absorption spectra of single polypeptide molecules are generally strongly broadened than those obtained for molecular crystals, pump-probe measurements are used to get further insight.

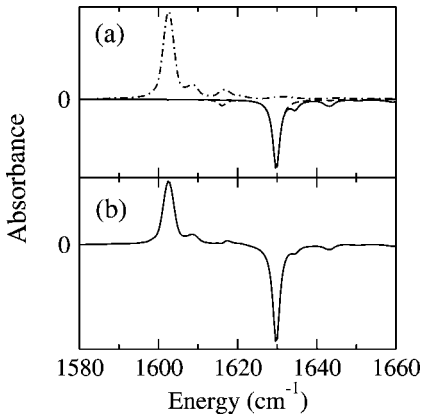

FIG. 9. (a) Components of the frequency dispersed differential TAS for the chain of ten amide units: ground-state bleaching signal (solid line), stimulated emission signal (dashed line), and excited-state absorption signal (dash-dotted line). (b) The total frequency dispersed differential TAS.

Experimental pump-probe data of the amide I mode of an α-helix have been reported in Ref. 35. The measured spectrum displays a negative band at a frequency below 1650 cm^{-1} and a redshifted positive band (Fig. 3 of Ref. 35). The position and relative height of these bands are in rather close agreement with our calculations [cf. Fig. 9(b)]. Since our model is based on a certain simplification of the real helical structure, it is hardly possible to achieve quantitative agreement with measurements. However, we believe that the key effects are correctly reproduced by our calculations.

Yet another motivation of our study is the pump-probe measurement performed recently in Ref. 7 for the N–H absorption band of the α helix. Respective specification of the model and numerical results will be presented soon.[36]

VI. CONCLUSIONS

In this paper, an accurate quantum-dynamical description has been used in order to study the linear and nonlinear infrared absorption spectra for the C=O stretching mode of α-helical polypeptides. A linear chain of ten amide units has been used as a model system. The multiexciton expansion of the model Hamiltonian was carried out to reduce the computational effort. The accuracy has been tested against the full-dimensional calculations based on the MCTDH method. Exciton probability distributions for the self-trapped exciton states were obtained from the adiabatic exciton approximation and using the full exciton-chain vibrational wave function. Comparison of calculated linear absorption spectra with the result obtained from the adiabatic exciton model indicates the importance of nonadiabatic effects in the amide exciton dynamics. The differential transient absorption signal of a sequential pump-probe experiment has been calculated for the first time using the full exciton-chain vibrational wave function, and the spectral response of self-trapped two-exciton states has been identified.

ACKNOWLEDGMENTS

Financial support of the Deutschen Forschungsgemeinschaft through Project Ma 1356/8-1 and Sfb 450 is gratefully acknowledged.

APPENDIX A: MULTIEXCITATION MATRIX ELEMENTS OF THE HAMILTONIAN

Before presenting all matrix elements of interest we shortly specify the parameters of the Morse potential used to account for the anharmonicity of the local amide vibration. Respective potentials $V_m(Q_m)$ have been introduced in relation to the specification of the Hamiltonian, Eq. (2), of all amide units. We neglect the site index and denote the potential as

$$V(Q) = E_d(e^{-2\alpha Q} - 2e^{-\alpha Q}). \tag{A1}$$

The coordinate Q is dimensionless and defined in a way that the kinetic energy operator reads $\hbar\omega_0 d^2/dQ^2$. The prefactor is taken as the oscillator frequency obtained from the harmonic approximation of the amide potential V_m. With respect to standard mass-weighted normal-mode coordinate q we have $Q=\sqrt{2\omega_0/\hbar}q$. The stationary eigenvalue problem for an isolated amide oscillator has been written down in Eq. (6). According to the Morse potential approximation of V_m, the spectrum reads $E_\mu=-E_d[1-\sqrt{\hbar\omega_0\alpha^2/E_d}(\mu+1/2)]^2$.

We introduce the energy ΔE_{01} of $(\mu=0\rightarrow\mu=1)$ transition, the anharmonicity A, and the frequency ω_0 of small oscillations as follows:

$$\Delta E_{01} = E_1 - E_0 = 2\sqrt{\hbar\omega_0\alpha^2}(\sqrt{E_d} - \sqrt{\hbar\omega_0\alpha^2}), \tag{A2}$$

$$A = \tfrac{1}{2}((E_1 - E_0) - (E_2 - E_1)) = \hbar\omega_0\alpha^2, \tag{A3}$$

$$\omega_0 = 4E_d\alpha^2/\hbar. \tag{A4}$$

One may express the parameters of the Morse potential through the experimentally accessible quantities ΔE_{01} and A as follows:

$$\alpha = \sqrt{A/(\hbar\omega_0)}, \tag{A5}$$

$$E_d = (\Delta E_{01} + 2A)^2/(4A). \tag{A6}$$

In order to determine the various multiexcitation matrix elements of the complete Hamiltonian in the subsequent section, we present some Morse oscillator states matrix elements of Q and Q^2. Those are real and we write:

$$Q^n_{\mu\nu} = \langle\chi_\mu|Q^n|\chi_\nu\rangle. \tag{A7}$$

Analytical expressions may be found in Refs. 37 and 38. Each matrix element can be defined in terms of the ratio E_d/A using the dimensionless parameter $k=2\sqrt{E_d/\hbar\omega_0\alpha^2}=2\sqrt{E_d/A}$ (cf. Ref. 38). Table II shows the values of the matrix elements (A7) for the anharmonic C=O stretching mode and for the harmonic oscillator as a reference case $(A=0)$.

TABLE II. Matrix elements of Morse oscillator states corresponding to the anharmonic C=O normal mode of the amide unit. Values for harmonic oscillator (HO) states are also given for reference.

Matrix element	C=O mode	HO
Q_{00}	0.1162	0.0000
Q_{11}	0.3509	0.0000
Q_{22}	0.5890	0.0000
Q_{01}	1.0030	1.0000
Q_{12}	1.4227	1.4142
Q_{02}	−0.0550	0.0000
Q^2_{00}	1.0225	1.0000
Q^2_{11}	3.1624	3.0000
Q^2_{22}	5.4473	5.0000
Q^2_{01}	0.3898	0.0000
Q^2_{12}	1.1130	0.0000
Q^2_{02}	1.3968	1.4142

1. Intramanifold matrix elements

In the following we list the matrix elements of the basic Hamiltonian H, Eq. (1), with the various singly and doubly excited states introduced in Sec. II B (note also the specifications of the model introduced in Sec. III A). The ground-state matrix element given in Eq. (16) is simply obtained as

$$\langle 0|H_{\rm mol}|0\rangle = \hat{T}_{\rm vib} + \mathcal{E}_0(x). \tag{A8}$$

Matrix elements with respect to singly excited states read [cf. Eq. (17)]

$$\langle\phi_m|H_{\rm mol}|\phi_n\rangle = \delta_{m,n}(\hat{T}_{\rm vib} + \mathcal{E}_0(x) + E_1 - E_0 + w_{m1}(x) - w_{m0}(x)) - (1-\delta_{m,n})(\delta_{m-1,n} + \delta_{m,n-1})J_1, \tag{A9}$$

where

$$J_1 = J\langle\phi_m|Q_mQ_{m-1}|\phi_{m-1}\rangle = J(Q_{10})^2. \tag{A10}$$

To obtain the Hamiltonian H_2 the following matrix elements are needed:

$$\langle\tilde{\phi}_{m,n}|H_{\rm mol}|\tilde{\phi}_{m,n}\rangle = \delta_{m,n}(\hat{T}_{\rm vib} + \mathcal{E}_0(x) + E_2 - E_0 + w_{m2}(x) - w_{m0}(x)) + (1-\delta_{m,n})(2E_1 - 2E_0 + w_{m1}(x) - w_{m0}(x) + w_{n1}(x) - w_{n0}(x)), \tag{A11}$$

as well as

$$\langle\tilde{\phi}_{k,l}|H_{\rm mol}|\tilde{\phi}_{m,n}\rangle = \delta_{m,k}\delta_{n,l}\langle\tilde{\phi}_{m,n}|H_{\rm mol}|\tilde{\phi}_{m,n}\rangle - (\delta_{m,n}\delta_{k,m}\delta_{k,l-1} + \delta_{m,n}\delta_{l,m}\delta_{k,l-1} + \delta_{k,l}\delta_{k,m}\delta_{m,n-1} + \delta_{k,l}\delta_{k,n}\delta_{m,n-1})J_2 - (\delta_{k,m}\delta_{l,n-1} + \delta_{k,m}\delta_{l-1,n} + \delta_{l,n}\delta_{k-1,m} + \delta_{l,n}\delta_{k,m-1})(1-\delta_{k,l})(1-\delta_{m,n})J_1, \tag{A12}$$

where $J_2=JQ_{21}Q_{10}$. In the foregoing equations we neglected all terms which disappear at the absence of the local amide mode anharmonicity. Such terms contain the off-resonant matrix elements of Q or Q^2 and they are typically small in comparison with the corresponding resonant matrix elements (cf. Table II). However, for the parts of the Hamiltonian $H_{1,0}$, $H_{2,1}$, and $H_{2,0}$ which describe the coupling between manifolds of singly and doubly excited states, as well as the amide ground state the off-resonant terms become important.

2. Intermanifold matrix elements

Here we present the matrix elements of the coupling terms between different manifolds of excited states. Couplings between the ground state and the manifold of singly excited states are described by

$$\langle \phi_m | H_{\mathrm{mol}} | 0 \rangle = -((1-\delta_{m,1})+(1-\delta_{m,N}))JQ_{00}Q_{10} + (1-\delta_{m,1})\frac{\chi}{2}Q_{10}^2(x_m - x_{m-1}). \tag{A13}$$

The two-exciton manifold and the exciton ground state are coupled via

$$\langle \tilde{\phi}_{m,n} | H_{\mathrm{mol}} | 0 \rangle = -\delta_{m+1,n}J(Q_{10})^2 - \delta_{m,n}((1-\delta_{m,1}) + (1-\delta_{m,N}))JQ_{20}Q_{00} + \delta_{m,n}(1-\delta_{m,1}) \times \frac{\chi}{2}Q_{20}^2(x_m - x_{m-1}). \tag{A14}$$

The coupling between the two- and single-exciton manifolds reads

$$\langle \tilde{\phi}_{m,n} | H_{\mathrm{mol}} | \phi_k \rangle = -\delta_{m,n}\delta_{m,k}((1-\delta_{m,1})+(1-\delta_{m,N}))JQ_{21}Q_{00} - \delta_{m,n}(\delta_{m,k+1}+\delta_{m+1,k})JQ_{20}Q_{10} + \delta_{m,n}\delta_{m,k}(1-\delta_{m,1})\frac{\chi}{2}Q_{21}^2(x_m - x_{m-1}) - \delta_{m+1,n}(\delta_{m,k}+\delta_{n,k})JQ_{11}Q_{10} - \delta_{m,k}(1-\delta_{m,n})(1-\delta_{m+1,n})(2-\delta_{n,N})JQ_{00}Q_{10} - \delta_{n,k}(1-\delta_{m,n})(1-\delta_{m+1,n})(2 - \delta_{m,1})JQ_{00}Q_{10} + (1-\delta_{m,n})(1-\delta_{m,1})\delta_{n,k}\frac{\chi}{2}Q_{10}^2(x_m - x_{m-1}) + (1-\delta_{m,n})\delta_{m,k}\frac{\chi}{2}Q_{10}^2(x_n - x_{n-1}). \tag{A15}$$

Finally, we mention the respective matrix elements of the dipole operator entering the molecule radiation-field coupling, Eq. (5) [note also Eq. (24)]. We obtain

$$\langle \phi_m | \hat{\boldsymbol{\mu}} | 0 \rangle = \mathbf{d}_1, \tag{A16}$$

$$\langle \tilde{\phi}_{m,n} | \hat{\boldsymbol{\mu}} | \phi_k \rangle = \delta_{m,n}\delta_{k,m}\mathbf{d}_2 + (1-\delta_{m,n})(\delta_{k,m}+\delta_{k,n})\mathbf{d}_1, \tag{A17}$$

with the abbreviations for the transition dipole moments ($\Delta\boldsymbol{\mu}_m \equiv \Delta\boldsymbol{\mu}$)

$$\mathbf{d}_1 = \Delta\boldsymbol{\mu}Q_{10}, \tag{A18}$$

$$\mathbf{d}_2 = \Delta\boldsymbol{\mu}Q_{21}. \tag{A19}$$

[1] P. Hamm, M. Lim, and R. M. Hochstrasser, J. Phys. Chem. B **102**, 6123 (1998).
[2] S. Mukamel, Annu. Rev. Phys. Chem. **51**, 691 (2000).
[3] S. Mukamel and R. M. Hochstrasser, in Multidimensional Spectroscopy, special issue of, Chem. Phys. **266**, 1 (2001).
[4] A. M. Moran, S.-M. Park, and S. Mukamel, J. Chem. Phys. **118**, 9971 (2003).
[5] A. M. Moran, S.-M. Park, J. Dreyer, and S. Mukamel, J. Chem. Phys. **118**, 3651 (2003).
[6] A. C. Scott, Phys. Rep. **217**, 1 (1992).
[7] J. Edler, R. Pfister, V. Pouthier, C. Falvo, and P. Hamm, Phys. Rev. Lett. **93**, 106405 (2004).
[8] J. Edler and P. Hamm, Phys. Rev. B **69**, 214301 (2004).
[9] J. Edler, P. Hamm, and A. C. Scott, Phys. Rev. Lett. **88**, 067403 (2002).
[10] D. W. Brown and Z. Ivic, Phys. Rev. B **40**, 9876 (1989).
[11] A. S. Davydov and N. I. Kisluka, Phys. Status Solidi B **59**, 465 (1973).
[12] W. Förner, Phys. Rev. A **44**, 2694 (1991).
[13] W. Förner, J. Phys.: Condens. Matter **3**, 3235 (1991).
[14] W. Förner, J. Phys.: Condens. Matter **4**, 1915 (1991).
[15] V. Pouthier, Phys. Rev. E **68**, 021909 (2003).
[16] V. Pouthier and C. Falvo, Phys. Rev. E **69**, 041906 (2004).
[17] C. Falvo and V. Pouthier, J. Chem. Phys. **123**, 184710 (2005).
[18] J. Antony, B. Schmidt, and C. Schütte, J. Chem. Phys. **122**, 014309 (2005).
[19] X. Wang, D. W. Brown, and K. Lindenberg, Phys. Rev. Lett. **62**, 1796 (1989).
[20] L. Cruzeiro-Hansson and S. Takeno, Phys. Rev. E **56**, 894 (1997).
[21] H.-D. Meyer, U. Manthe, and L. S. Cederbaum, Chem. Phys. Lett. **165**, 73 (1990).
[22] H.-D. Meyer and G. A. Worth, Theor. Chem. Acc. **109**, 251 (2003).
[23] U. Manthe, H.-D. Meyer, and L. S. Cederbaum, J. Chem. Phys. **97**, 3199 (1992).
[24] M. H. Beck, A. Jäckle, G. A. Worth, and H.-D. Meyer, Phys. Rep. **324**, 1 (2000).
[25] D. V. Tsivlin and V. May, Chem. Phys. Lett. **408**, 360 (2005).
[26] V. May and O. Kühn, *Charge and Energy Transfer Dynamics in Molecular Systems*, 2nd ed. (Wiley-VCH, Berlin, 2004).
[27] B. Brüggemann, D. V. Tsivlin, and V. May, in *Ultrafast Exciton Dynamics in Molecular Systems*, Proceedings of the Paris Conference on Quantum Dynamics, edited by M. Burghardt and D. Micha (in press).
[28] W. M. Zhang, T. Meier, V. Chernyak, and S. Mukamel, J. Chem. Phys. **108**, 7763 (1998).
[29] D. M. Alexander and J. A. Krumhansl, Phys. Rev. B **33**, 7172 (1986).
[30] G. A. Worth, M. H. Beck, A. Jäckle, and H.-D. Meyer, The MCTDH Package, Version 8.2, 2000; H.-D. Meyer, The MCTDH Package, Version 8.3, 2002, see http://www.pci.uni-heidelberg.de/tc/usr/mctdh/
[31] S. Mukamel, *Principles of Nonlinear Optical Spectroscopy* (Oxford University Press, New York, 1995).
[32] L. Seidner, G. Stock, and W. Domcke, J. Chem. Phys. **103**, 3998 (1995).
[33] H. Torii and M. Tasumi, J. Chem. Phys. **96**, 3379 (1992).
[34] C. Falvo and V. Pouthier, J. Chem. Phys. **122**, 014701 (2005).
[35] C. Fang, J. Wang, Y. S. Kim, A. K. Charnley, W. Barber-Armstrong, A. B. Smith III, S. M. Decatur, and R. M. Hochstrasser, J. Phys. Chem. B **108**, 010415 (2004).
[36] D. V. Tsivlin and V. May, J. Chem. Phys. (to be published).
[37] J. A. C. Gallas, Phys. Rev. A **21**, 1829 (1980).
[38] D. Malzahn and V. May, Chem. Phys. **197**, 205 (1995).